Journal of Controlled Release 398 (2026) 115190

Contents lists available at ScienceDirect

Journal of Controlled Release

journal homepage: www.elsevier.com/locate/jconrel

Simple hybrid predictive model for point-of-care pharmaceutical tablet disintegration

Chi Ki Leung [a], Prince Bawuah [a,1], Nicolas Spiesshofer [b], Andreas Kottlan [c], Jeremy J. Baumberg [b], J. Axel Zeitler [a,*]

[a] Department of Chemical Engineering and Biotechnology, University of Cambridge, Philippa Fawcett Drive, Cambridge, CB3 0AS, United Kingdom
[b] NanoPhotonics Centre, Cavendish Laboratory, Department of Physics, JJ Thompson Avenue, University of Cambridge, Cambridge, CB3 0US, United Kingdom
[c] Research Center Pharmaceutical Engineering GmbH, Inffeldgasse 13/2, 8010 Graz, Austria

ARTICLE INFO

Keywords:
Porosity
Disintegration
Predictive modelling
Hybrid model
Oral solid dosage
Stability
Real-time release testing

ABSTRACT

Ensuring the consistent disintegration performance of immediate-release oral solid dosage (OSD) forms throughout their shelf life is critical for therapeutic efficacy, yet predicting point-of-care performance from manufacturing data remains a significant challenge. Current predictive approaches often rely on empirical correlations or high-dimensional black-box models that lack mechanistic insight and longitudinal validity. To address this, a simple hybrid model that predicts longitudinal disintegration times $t_{\mathrm{disint},T}$ solely from at-line porosity measurements $f_{\mathrm{at-line}}$ is established. The framework is anchored in United States Pharmacopoeia <701> standards to ensure regulatory compliance and reproducibility, while maintaining an architecture that is agnostic to the specific porosity characterisation technique. Utilising a five-year real-time stability dataset with different formulations and tablet geometries, global models are established and demonstrate exceptional predictive accuracy ($R^2 > 0.92$) across all longitudinal time points. The operating range lies in $f_{\mathrm{at-line}} \in [0.1, 0.3]$, which is the typical porosity range of pharmaceutical OSDs. The model's longitudinal validity is predicated on the physicochemical stability of the formulation, allowing the model parameters to serve as quantitative indicators in stability assessments. The simplicity and adaptability of this mechanistically grounded model offer a pragmatic path to demonstrating dosage form efficacy at the point-of-care, providing a robust alternative to traditional, destructive end-point testing. By relating at-line structural attributes to long-term performance, this model facilitates Quality by Design in development, seamless technical transfer, and robust real-time release testing. Ultimately, this framework ensures that the rigorously designed quality standards are demonstrably preserved until the moment of patient administration.

1. Introduction

Immediate-release (IR) oral solid dosage (OSD) forms undergo rapid disintegration and subsequent dissolution upon contact with physiological fluids, typically within a window of 2.5 min to 10 min, to enhance drug bioavailability and to enable rapid onset of action [1–4]. For IR OSDs containing highly soluble active pharmaceutical ingredients (APIs), the International Conference on Harmonisation (ICH) Q6 A guideline stipulates that disintegration may replace dissolution testing, provided a definitive relationship between the two critical quality attributes (CQAs) is established [5]. Disintegration time, therefore, forms one of the significant criteria in the Quality Target Product Profile (QTPP) of IR formulations.

Liquid transport initiates the disintegration of pharmaceutical tablets [6]. Fast liquid transport can enable disintegration via a single-event burst release of the tablet, whereas slow penetration leads to disintegration via gradual surface erosion [6]. The dynamics of liquid transport are often described by the Lucas–Washburn equation, which relates the rate of penetration to the pore geometry, surface tension, fluid viscosity and contact angle [7,8]. The structural integrity of a pharmaceutical tablet is maintained by various interparticle forces, including solid bridges, hydrogen bonds, van der Waals forces and mechanical interlocking [2,7]. These cohesive forces must be overcome for disintegration to occur and are facilitated by disintegrants mainly via swelling and shape recovery [2,4,7]. Swelling refers to the 3-D expansion of the particle, whereas shape recovery only involves particle ex-

* Corresponding author.
E-mail address: jaz22@cam.ac.uk (J.A. Zeitler).
[1] Current address: Menlo Systems GmbH, Bunsenstraße 5, 82152 Martinsried, Germany

https://doi.org/10.1016/j.jconrel.2026.115190
Received 14 May 2026; Received in revised form 14 July 2026; Accepted 17 July 2026
Available online 24 July 2026

pansion in the axial direction based on elastic strain recovery [6,9]. Superdisintegrants, such as sodium starch glycolate (SSG) and croscarmellose sodium (CCS), primarily act through swelling, while starch and crospovidone (XPVP) operate primarily via shape recovery. The effectiveness of disintegrants is heavily influenced by the properties of other excipients and active pharmaceutical ingredients (APIs) in the tablet. Fillers, binders, and diluents typically account for a significant fraction of a formulation and thus dictate the overall disintegration mechanisms. The mechanisms are largely split into wettability-controlled, swelling-controlled and dissolution-controlled [10].

In addition to the Lucas–Washburn model, more sophisticated models have been developed to describe liquid transport kinetics for swelling IR pharmaceutical tablets [11]. Discrete Element Method (DEM) and Finite Difference Method (FDM) approaches have also been implemented to simulate particle detachment and liquid diffusion, respectively, to better understand the disintegration process [12–14]. To address the complex interplay between critical material attributes and process parameters in disintegration, machine learning models have been used to predict disintegration times [15–20]. Despite achieving accuracies and R^2 up to around 85 % and 0.98, respectively [15–17], these models require vast datasets and provide limited physical interpretability. Mechanistic frameworks such as the Representative Capillary Evolution Model (RCEM) and the Dynamic Void Fraction Evolution Model (DVFEM) have since been proposed to physically model the changing pore structure during liquid transport and disintegration [21].

The mechanistic models discussed above indicate that the tablet microstructure is an important contributor to disintegration. Specific microstructure properties include the effective pore radius, tortuosity and constriction factor. These factors are often challenging to quantify, and so the overall porosity becomes a convenient yet critical quality attribute to describe the tablet microstructure and inform disintegration performance [2,11,14,22–27]. Riippi et al. [22] established that a lower compression force, hence higher porosity, results in shorter tablet disintegration time.

Pharmaceutical tablet porosity has thus been rigorously integrated into Quality by Design (QbD) and real-time release testing (RTRT) frameworks [28–37]. Recent advancements in process analytical technology (PAT) have enabled the development of soft sensors that link rapid, non-destructive porosity measurements to disintegration times via empirical calibration models [38,39]. While these PATs and models provide valuable immediate feedback, the critical clinical dimension on the temporal evolution of the dosage form throughout the shelf life is yet to be considered.

From a clinical perspective, the tablet disintegration time at the point-of-care, which may occur months or years after storage, is of paramount importance compared to the disintegration performance predicted at the manufacturing line. For a predictive model to be impactful and maximised for patient safety and therapeutic efficacy, it must confidently inform the pharmaceutical tablet's performance throughout its intended shelf life. This leaves a gap in drug product development and pharmaceutical secondary manufacturing for models that can translate at-line structural measurements into point-of-care performance metrics.

The present study addresses this gap by establishing a simple hybrid model designed to predict disintegration times $t_{\mathrm{disint},T}$ at different time points T of the shelf life based on at-line porosity measurements $f_{\mathrm{at-line}}$. $t_{\mathrm{disint},T}$ is defined according to the United States Pharmacopoeia (USP) Chapter ⟨701⟩ Disintegration. By anchoring the model in the USP standard, the model's reproducibility and regulatory compliance can be ensured. Crucially, the model is agnostic to the specific porosity PAT, provided the characterisation is valid and accurate. The model parameters function as quantitative indicators of the formulation's physicochemical stability, which directly underpins the model's longitudinal validity. The simplicity of the model enables easy adaptation to different formulations, straightforward technical transfer, and efficient implementation in drug product development, manufacturing, and life cycle management. By shifting the focus from immediate characterisation to longitudinal prediction, a more robust assurance is provided on the product safety and efficacy at the point-of-care. This moves beyond the limitations of traditional end-point testing and stability assessments.

2. Experimental methods

This study is based upon the materials and methods from Bawuah et al. [38] and Maclean et al. [40]. Readers are referred to the two publications for details of the pharmaceutical tablet manufacturing and material characterisation.

2.1. Materials

Two formulations with the same excipient composition but different APIs were investigated. The formulations contained microcrystalline cellulose (MCC) (Avicel PH-102, FMC Europe NV, Belgium) (39.1 wt %), lactose anhydrous (Supertab21AN, DFE pharma, Germany) (46.9 wt %), CCS (DuPont Nutrition, USA) (3.0 wt %), magnesium stearate (Fisher Scientific, USA) (1.0 wt %) and an API of either ibuprofen (BLD Pharmatech, China) or indomethacin (Sigma-Aldrich Company Ltd., UK) (10.0 wt %).

The true densities of the two APIs were measured with a gas pycnometer (MicroUltrapyc 1200e, Quantachrome Instruments, Graz, Austria) with nitrogen. The true density of the formulation $\rho_{\mathrm{true,formulation}}$ is determined by Sun [41] and Maclean et al. [40]:

$$\rho_{\mathrm{true,formulation}} = \left(\sum_{i}^{N} \frac{x_{\mathrm{i}}}{\rho_{\mathrm{true,i}}} \right)^{-1} \tag{1}$$

where x_{i} and $\rho_{\mathrm{true,i}}$ are the mass fraction and the true density of a component.

2.2. Pharmaceutical tablets

10 mm diameter biconvex cylindrical tablets with and without debossing were made for each of the two formulations. Four types of tablets thus resulted. Each tablet weighed around 400 mg and the text "TPI" was inscribed on one biconvex surface of the tablet as debossing, where relevant. The mass M, height H and diameter D of each tablet were measured by a mass balance (Fisher Scientific, Illkirch-Graffenstaden, France) and a micrometer (Sealey Digital External Micrometer 0–25 mm; Rapid Electronics Limited, Colchester, UK), respectively. For each tablet type, five tablet batches with different nominal porosities f_{nom} were produced. The mean at-line nominal porosities across all investigated batches are $f_{\mathrm{nom,at\text{-}line}} = 0.08, 0.12, 0.16, 0.21$ and 0.25. f_{nom} was determined by

$$f_{\mathrm{nom}} = 1 - \frac{\rho}{\rho_{\mathrm{true,formulation}}} = 1 - \frac{M}{V \rho_{\mathrm{true,formulation}}} \tag{2}$$

where ρ is the tablet density and the tablet volume V is calculated based on the biconvex cylindrical geometry:

$$V = \frac{2\pi H_{\mathrm{cap}}^2}{3}(3r_{\mathrm{cap}} - H_{\mathrm{cap}}) + \frac{\pi D^2}{4}(H - 2H_{\mathrm{cap}}) \tag{3}$$

with H_{cap} and r_{cap} being the height and radius of the biconvex cap.

2.3. Characterisation scheme

Hereafter, a tablet set refers to a tablet type at a specific measurement time point. Table 1 summarises the number of pharmaceutical tablets characterised by each method across the sets. Measurements at year 0 are the at-line measurements.

2.4. Terahertz porosity measurements

THz-TDS measurements in a nitrogen-purged environment (TeraPulse 4000, TeraView Ltd., Cambridge, UK) were conducted for each

Table 1
Tablet counts across sample sets and characterisation methods. DT refers to USP <701> disintegration testing.

Tablet set			Number of tablets characterised in each method		
	Debossing	Year	Nominal porosity	Terahertz porosity	DT
Ibuprofen biconvex tablets	Yes	0	39	39	0
	Yes	3	15	15	0
	Yes	4	15	15	15
	Yes	5	24	24	24
	No	0	44	44	30
	No	3	14	14	0
	No	4	14	14	14
Indomethacin biconvex tablets	Yes	0	44	44	0
	Yes	3	15	15	0
	Yes	4	15	15	15
	Yes	5	29	29	29
	No	0	45	45	30
	No	3	15	15	0
	No	4	15	15	15

pharmaceutical tablet. A baseline measurement of an empty beam path accompanies each tablet measurement. Details of the terahertz data processing are described in Appendix A. The terahertz porosity f_{THz} and frequency ν-dependent complex effective refractive index spectra $\hat{n}_{\mathrm{eff}}(\nu)$ for each tablet, and the complex solid refractive index spectra $\hat{n}_{\mathrm{solid}}(\nu)$, a material property of the formulation, for each tablet set are determined.

2.5. Disintegration testing

USP ⟨701⟩ disintegration testing was conducted with a standard disintegration tester (DT50, SOTAX AG, Switzerland). Pharmaceutical tablets were placed on the basket rack which moves at 30 strokes per minute. 900 mL tap water at 37 °C was utilised in the test.

2.6. Storage

Individual pharmaceutical tablets were placed in sealed polyethylene sample bags, which were then grouped by batch and type into secondary and tertiary sealed polyethylene bags.

The tablets were stored at ambient temperature (~ 21 °C), pressure (~ 1 bar) and humidity (~ 30 % relative humidity) to simulate typical storage conditions. Tablets were only removed from the polyethylene bags during measurements.

2.7. Fourier transform infrared-attenuated total reflectance spectroscopy

To confirm the stability of ibuprofen, powder samples of the five-year-old ibuprofen formulation were taken from the top and side of the container. The powder samples were then respectively measured with Fourier transform infrared-attenuated total reflectance (ATR-FTIR) spectroscopy (Shimadzu IRTracer-100 and QATR-10 accessory with diamond crystal, Shimadzu UK Limited, UK). The powder samples were loaded onto the ATR diamond crystal and mechanically compressed. Measurements were taken at a resolution of $4\,\mathrm{cm}^{-1}$, averaged over 50 scans, and referenced to the clean diamond crystal. For comparison, a freshly made ibuprofen formulation and pure ibuprofen were also measured with ATR-FTIR spectroscopy.

3. Simple predictive model for point-of-care disintegration

Consider two identical unit volumes filled with particles of the same particle size distribution and ρ_{true}. One of the unit volumes contains a greater mass, so it has a higher density and requires a longer disintegration time. This can be expressed in the form of a differential equation where

$$\frac{\mathrm{d}t_{\mathrm{disint}}}{\mathrm{d}\rho} = a\rho^{b} \tag{4}$$

where t_{disint} is the disintegration time, ρ is the density of the unit volume, and a and b are model parameters relating to the properties of the particles and disintegration medium. The boundary condition can be established from the case of $\rho = 0\,\mathrm{kg\,m^{-3}}$, where no mass is present in the unit volume and so t_{disint} must be 0 s. Integrating Eq. (4) and substituting the boundary condition leads to

$$t_{\mathrm{disint}} = \frac{a}{b+1}\rho^{b+1} \tag{5}$$

Based on the relationship between porosity f and ρ (Eq. (2)), Eq. (5) can be alternatively expressed as

$$t_{\mathrm{disint}} = k'(1-f)^{r'} \tag{6}$$

where $k' = \frac{a}{b+1}\rho_{\mathrm{true}}^{b+1}$ and $r' = b+1$.

The exponent r' governs the non-linear dependency of t_{disint} on the solid fraction $(1-f)$ in Eq. (6) and indirectly regulates the non-linear relationship of the change in t_{disint} with ρ in Eq. (4). This demonstrates the material and formulation sensitivity of r', which is linked to the mass transport mechanisms and the energetic threshold required for bond breakage. The tablet geometry, particle size distribution, surface area, surface morphology, inter-particle bond strength, strain recovery, particle swelling, solubility, hydrophilicity and molecular mobility are possible contributors to r'. In contrast, the pre-exponential factor k', which is a function of r' and rate constant a, is defined here as the intrinsic disintegration constant. While k' incorporates the material properties described by r', it further accounts for the dynamic fluid–solid interactions that dictate the rate of liquid ingress and subsequent particle detachment. The interactions are determined by the pore architecture such as pore radius, connectivity, and tortuosity, and the physicochemical properties of the disintegration medium, such as surface tension, contact angle, and viscosity. By identifying f as the primary governing CQA for t_{disint}, this framework allows for a significant reduction in dimensionality. All auxiliary factors, ranging from molecular mobility to macroscopic solubility, are effectively and collectively captured by the parameters k' and r', enabling a robust yet simple predictive model for longitudinal performance.

Up to this point, t_{disint} and f correspond to the same time point T during the shelf life of the pharmaceutical tablet. To relate the disintegration time at a specific time point T in the shelf life $t_{\mathrm{disint},T}$ with the at-line porosity $f_{\mathrm{at-line}}$, an apparent option is to establish a time-dependent relationship between the porosity at time point T of the shelf life and $f_{\mathrm{at-line}}$. However, amongst the investigated tablets and available terahertz porosity data, the change in porosity with respect to the at-line porosity, which is measured at year 0, consistently aggregated around $\Delta f_{\mathrm{THz}} = [0.01, 0.04]$ over time (Appendix B Fig. B.1, B.2). The fractional change in porosity with respect to the at-line porosity $\frac{\Delta f_{\mathrm{THz}}}{f_{\mathrm{THz,at-line}}}$ remains consistent over time, with tablets without debossing showed less distinction for different $f_{\mathrm{THz,at-line}}$ (Appendix B Fig. B.1, B.2). More importantly, $f_{\mathrm{THz,at-line}}$ has a greater impact on

Table 2
Model parameters for each tablet set and for the three global models. R^2 and RMSE are derived based on the training tablets' linear fit of $\ln(t_{disint})$ against $\ln(1 - f_{THz,at-line})$.

Tablet type					Model parameters				
	Debossing	Year	Number of training tablets	Number of testing tablets	R^2	RMSE (–)	r (–)	$\ln(k)$ (–)	k (s)
Models for each independent tablet set									
Ibuprofen biconvex tablets	Yes	4	15	–	0.984	0.171	15.2 ± 0.5	6.64 ± 0.11	764 ± 84
Ibuprofen biconvex tablets	Yes	5	24	–	0.982	0.157	16.1 ± 0.5	6.81 ± 0.09	909 ± 84
Ibuprofen biconvex tablets	No	0	30	–	0.964	0.241	16.9 ± 0.6	7.16 ± 0.12	1290 ± 152
Ibuprofen biconvex tablets	No	4	14	–	0.982	0.154	17.1 ± 0.7	7.00 ± 0.13	1100 ± 144
Indomethacin biconvex tablets	Yes	4	15	–	0.984	0.156	15.4 ± 0.5	7.05 ± 0.11	1150 ± 124
Indomethacin biconvex tablets	Yes	5	29	–	0.973	0.195	16.0 ± 0.5	7.12 ± 0.10	1240 ± 126
Indomethacin biconvex tablets	No	0	30	–	0.971	0.224	15.7 ± 0.5	7.17 ± 0.10	1300 ± 133
Indomethacin biconvex tablets	No	4	15	–	0.974	0.225	16.5 ± 0.8	7.26 ± 0.15	1430 ± 213
Global models									
Ibuprofen biconvex tablets	Yes	All	26	13	0.981	0.171	15.7 ± 0.4	6.72 ± 0.09	826 ± 74
Ibuprofen biconvex tablets	No	All	30	14	0.957	0.255	16.9 ± 0.7	7.09 ± 0.13	1200 ± 154
Indomethacin biconvex tablets	All	All	60	29	0.968	0.218	15.6 ± 0.4	7.09 ± 0.07	1200 ± 88

$t_{disint,T}$ (Section 4.1) than Δf_{THz} over time. Since all other material and structural factors are collectively represented by k' and r' (Eq. (6)) and the impact of Δf should not be substantial for a stable pharmaceutical product as in this study, it is therefore justifiable to integrate Δf_{THz} implicitly and dynamically into the model parameters to preserve the simple model architecture. This results in the model with parameters k and r:

$$t_{disint,T} = k(1 - f_{at-line})^r \tag{7}$$

The simplicity of the model (Eq. (7)) enables easy adaptation for a wide range of formulations, as well as implementation in drug product development and manufacture to predict point-of-care disintegration times based on at-line porosities. Should the model be applied to unstable pharmaceutical products, a case-by-case approach shall be applied to establish f, k' and r' (Eq. (6)) as functions of T in order to relate $t_{disint,T}$ to $f_{at-line}$. This is due to the varying significance of different time-dependent changes such as mechanical relaxation, water uptake and chemical degradation across formulations. Data-driven mathematical expressions of $f(T)$, $k'(T)$ and $r'(T)$ will enable a straightforward approach to dynamic predictions and the relatively simple model architecture to be maintained. The interpretation of the mathematical expressions would support the identification of CQAs and the critical mechanistic processes that contribute to the time-dependent changes, facilitating the development of more sophisticated mechanistic models on predicting point-of-care disintegration time.

The model (Eq. (7)) is valid for porosities measured by any accurate characterisation techniques. In this study, porosity f_{THz} is measured by terahertz time-domain spectroscopy (THz-TDS) since the technique's rapidity and non-destructiveness are desirable for at-line implementation. f_{THz} is shown to agree well with f_{nom} in Appendix B Fig. B.3 and in literature [30,38,39,42]. In addition, THz-TDS can provide further information on the pore and material properties of the tablet, which are discussed in Section 4.3 in relation to the interpretation of the model parameters.

4. Results and discussion

4.1. Model validation

The proposed hybrid model was first validated by fitting the linearised logarithmic form of Eq. (7) to each independent tablet set (Fig. 1):

$$\ln(t_{disint,T}) = r\ln(1 - f_{THz,at-line}) + \ln(k) \tag{8}$$

The linear logarithmic form facilitates robust evaluation of the model's goodness-of-fit. The resulting linear regressions yielded excellent R^2 and RMSE values, supporting the model theory and its applicability across different formulations and storage durations (Table 2).

The formulation dependency of the model parameters $\ln(k)$ and r (Section 3) is evidenced by their similarity (Table 2, Fig. 2), as 90 wt% of the two investigated formulations are identical. $\ln(k)$ and r remained consistent over time for each tablet type with the available data (Fig. 2).

The standard errors of $\ln(k)$ and r (Table 2, Fig. 2) are mathematically determined by the sample size, residual standard error, and the sum of squared differences between $\ln(1 - f_{THz,at-line})$ and its mean. Smaller sample sizes consistently yield wider, if not the same, standard errors within identical tablet types (Table 2, Fig. 2). This sample-size effect is particularly pronounced for the indomethacin biconvex tablets without debossing. Although the tablet sets from years 0 and 4 exhibit near-identical RMSEs, which share a similar derivation to the residual standard error, their sample sizes differ by a factor of two (Table 2). Hence, the sum of squared differences between $\ln(1 - f_{THz,at-line})$ and its mean are notably different across the two tablet sets, resulting in distinct standard errors in $\ln(k)$ and r (Table 2).

This confirms that the fluctuations in the standard errors of $\ln(k)$ and r are artefacts of the statistical treatment and sample size, rather than reflections of the physical changes within the tablets. The long-term invariance of $\ln(k)$ and r thus highlights the remarkable longitudinal stability of these formulations, which extends well beyond the typical shelf life of commercial pharmaceutical products. This temporal stability demonstrates that the underlying material properties and microstructural architecture governing disintegration did not undergo sufficient degradation or structural relaxation to alter the relationship between initial at-line porosity and long-term performance. Furthermore, the exceptional R^2 and RMSE values (Table 2) validate the hypotheses that $f_{THz,at-line}$ impacts t_{disint} much more significantly than Δf over time, and the parameters k and r effectively capture the subtle time-dependent structural changes observed in the porosity data (Section 3, Appendix B Fig. B.1).

This enables a robust mechanistic relationship between $t_{disint,T}$ and $f_{THz,at-line}$ to be flexibly established across formulations, demonstrating the model's adaptability. If $\ln(k)$ and r are not consistent over time within a tablet type and an one-way analysis of variance (ANOVA) test confirms these statistical distinctions, the tablets are considered unstable and the implicit treatment of Δf (Section 3) should be reviewed. Explicitly expressing f in Eq. (6) as a function of T and $f_{THz,at-line}$ in such cases will clarify the significance of structural relaxation for tablet instability and enable a more general predictive model to be established.

The ranges for $\ln(k)$ and r do not overlap between ibuprofen biconvex tablets with and without debossing (Fig. 2a, b). ANOVA tests with three degrees of freedom are thus performed for $\ln(k)$ and r respectively, resulting in F-statistics of 9.09 and 8.49, and p-values of 0.094 and 0.100. The p-values are greater than a 0.050 significance level, indicating debossing is not statistically significant in impacting

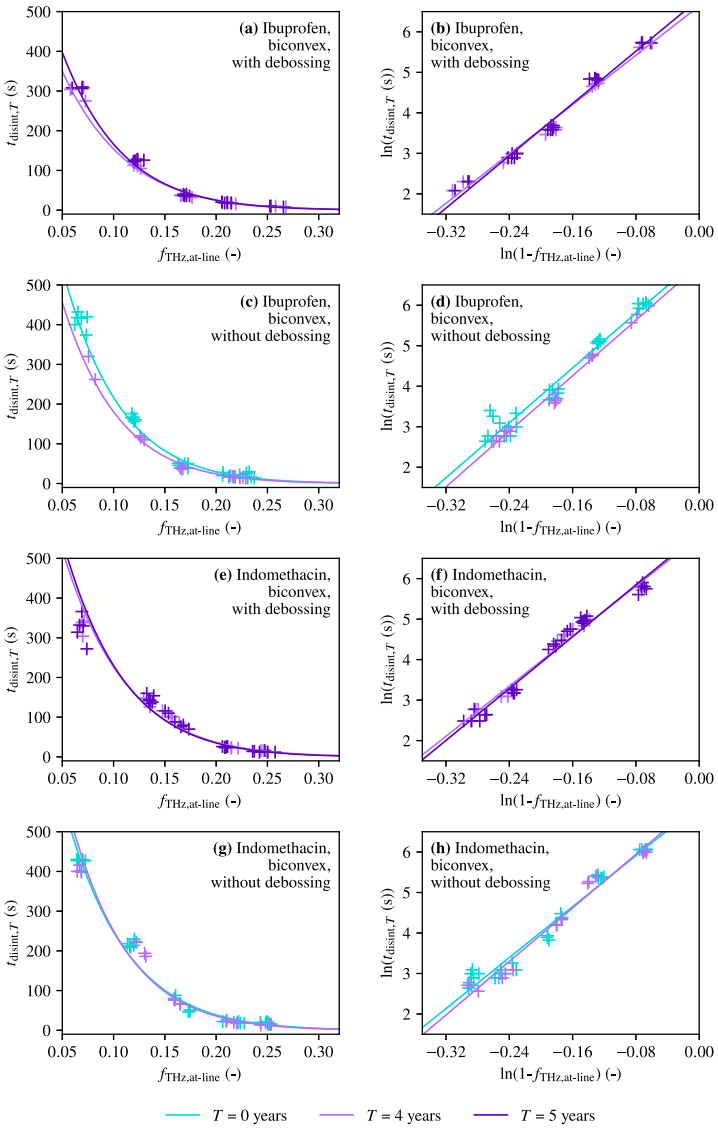

Fig. 1. Experimental and modelled disintegration times t_{disint} at different time points against the at-line porosity $f_{THz,at-line}$ in linear scale for ibuprofen biconvex tablets (a) with and (c) without debossing, and indomethacin biconvex tablets (e) with and (g) without debossing. Each data point corresponds to a unique tablet. (b, d, f, h) show the corresponding logarithmic transformations, demonstrating the models' linear fit.

the fitted model parameters and thus the disintegration mechanism. Nonetheless, the statistically minor disintegration difference due to debossing geometry in ibuprofen biconvex tablets can be attributed to the ~20-fold higher solubility of ibuprofen relative to indomethacin [43,44]. Debossing slightly increases the available surface area for dissolution, and more importantly, localised variations in density and interparticle forces facilitate liquid ingress, particle erosion, dissolution and thus disintegration. This is evidenced by the accelerated disintegration observed in debossed ibuprofen biconvex tablets compared to their counterparts without debossing, particularly at lower porosities where dissolution becomes a more prominent contributor to the disintegration process (Fig. 1a, c). Although a single disintegration model for all ibuprofen tablets regardless of debossing geometry and storage time is statistically viable, a more refined and conservative approach is adopted. Given the limited data in the one-way ANOVA tests and the varying factors contributing to disintegration, establishing separate global models for ibuprofen biconvex tablets with and without debossing ensures maximum stringency. For the indomethacin formulation, the overlapping ranges of $\ln(k)$ and r irrespective of debossing or storage time indicate that a single, global model can sufficiently describe disintegration performance (Fig. 2c, d).

4.2. Model universality and predictive robustness

Tablets within each set were randomly assigned into a training-to-testing ratio of 2:1 (Table 2) to establish the predictive power and adaptability of the three global models identified in Section 4.1, namely (i) ibuprofen biconvex tablets with debossing, (ii) ibuprofen biconvex tablets without debossing, and (iii) indomethacin biconvex tablets with and without debossing. Although the inherent logistical constraints of the multi-year stability study skewed the sample distribution towards earlier time points, the consistency of the $\ln(k)$ and r parameters observed over time (Section 4.1) justifies that the established global models remain unbiased.

The global models exhibited excellent fit to the training data (Table 2), successfully integrating $t_{disint,T}$ across all longitudinal time points and, additionally for indomethacin, across both debossing geometries. When applying the models to the respective independent testing sets, the observed $t_{disint,T}$ fell predominantly within the 95 % confidence

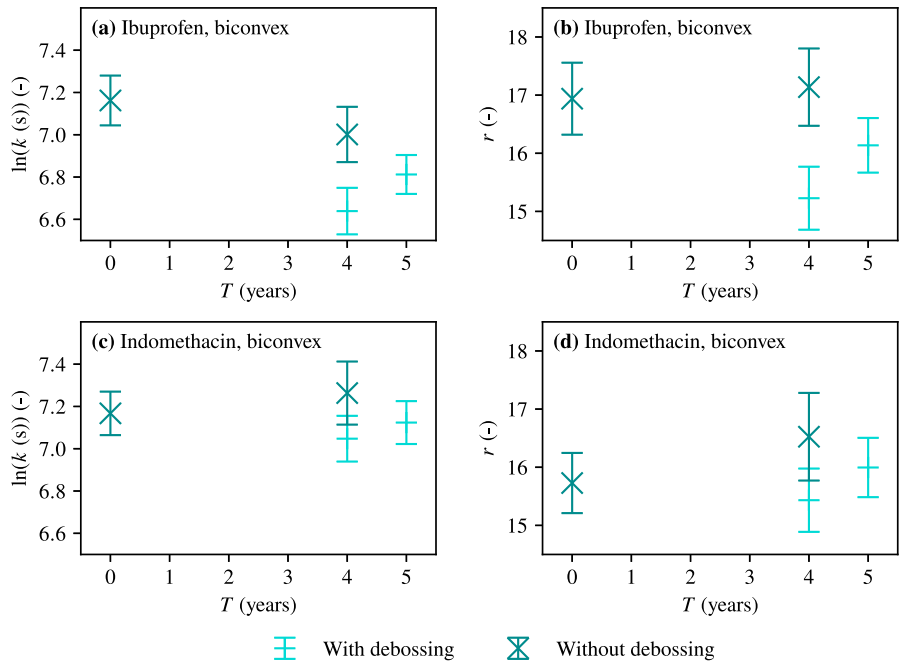

Fig. 2. Variation of the fitted model parameters (a, c) $\ln(k)$ and (b, d) r with time for (a, b) ibuprofen and (c, d) indomethacin biconvex tablets.

intervals and entirely within the 95 % prediction intervals (Fig. 3). R^2_{test} and $\text{RMSE}_{\text{test}}$ are determined for the independent testing sets against the respective models. R^2_{test} is slightly higher, if not comparable, to the training R^2, and $\text{RMSE}_{\text{test}}$ is systematically lower than the training RMSE across all three global models. The strong agreement between training and testing sets explicitly substantiates the predictive validity of the model and confirms the absence of overfitting. The model parameters $\ln(k)$ and r for these global configurations (Table 2) were consistent with the ranges observed in the corresponding individual tablet sets (Table 2), confirming that the global models accurately represent the underlying physical behaviour of the tablet sets. Notably, $\ln(k)$ and r remain distinct between the two ibuprofen models (Table 2). This reinforces the earlier conclusion (Section 4.1) that debossing introduces a fundamental change in the disintegration kinetics of ibuprofen biconvex tablets and necessitates a geometry-specific modelling approach.

Analysis of the predicted $t_{\text{disint,pred}}$ versus observed $t_{\text{disint,obv}}$ disintegration times revealed a high degree of agreement across the five-year study period and the tablet types (Fig. 4). The operating range of the model (Eq. (7)) is established to be $f_{\text{THz,at-line}} \in [0.1, 0.3]$, which matches the typical porosity range of commercial pharmaceutical OSD forms (Fig. 4b, e, h). The model demonstrates superior robustness within the operating range (Fig. 4b, e, h), achieving up to $\sim$ 50 % reduction in RMSE values relative to the complete dataset (Fig. 4a, d, g), despite a slight reduction in the R^2 values. Conversely, the model's validity diminishes at $f_{\text{THz,at-line}} < 0.1$ (Fig. 4c, f, i), where the observed disintegration times significantly lengthen and deviate from the predicted trend (Fig. 4c, f, i). For the excipient matrix (MCC/lactose anhydrous/CCS) in this study, disintegration is driven primarily by polymer swelling and liquid absorption. This is supported by comparing the disintegration mechanisms of MCC/lactose monohydrate/CCS, MCC/mannitol/CCS and the dissolution rate of lactose anhydrous, lactose monohydrate and mannitol [10,45–47]. However, a highly densified tablet matrix fundamentally alters these kinetics. At low porosities, the severely restricted pore space directly hinders initial liquid absorption, while the highly compressed matrix mechanically constrains the swelling capacity of MCC and CCS [47]. This structural inhibition suppresses the primary disintegration mechanisms, causing a significant increase in disintegration time that transcends the model's simple mechanistic basis. This provides evidence that the operating range lies within the optimal porosity range where liquid absorption is not impeded and expanding disintegrants can effectively exert force on neighbouring particles. The lower boundary $f_{\text{at-line}} = 0.1$ of the operating range does not limit the model's industrial utility, since manufacturing pharmaceutical tablets at $f < 0.1$ is practically challenging and often undesirable due to the risk of mechanical failure.

The model's adaptability is underscored by its ability to predict long-term disintegration performance from the at-line porosities of tablets with different formulations and geometries. The consistency and universality of the model over five years are direct consequences of the physical stability of the investigated formulations. As expected for a stable pharmaceutical product, the tablets do not undergo substantial structural relaxation over their shelf life (Appendix B Fig. B.1). Furthermore, the mean change in mass for all tablets, with respect to the mass acquired at-line, is 0.7 mg across all measured time points over five years. This indicates minimal water uptake and further substantiates the lack of significant physical changes. $f_{\text{at-line}}$ thus remains the primary governing CQA with profound predictive value for point-of-care disintegration performance.

A sensitivity analysis was performed to evaluate the impact of $f_{\text{at-line}}$ variations on the model's non-linear power-law architecture. While a porosity deviation of ± 0.01 yields predicted $t_{\text{disint},T}$ within the 95 % confidence interval, an increased deviation of ± 0.03 pushes the predictions to or beyond the boundaries of the 95 % prediction interval (Fig. 5). Across half of the operating range ($f_{\text{THz}} \in [0.1, 0.3]$), a ± 0.03 fluctuation in $f_{\text{THz,at-line}}$ introduces absolute errors in $t_{\text{disint},T}$ that exceed one-third of the theoretical predicted values (Fig. 5). These findings emphasise the exceptional sensitivity of the hybrid predictive model. High-precision training data and accurate at-line porosity characterisation are thus paramount to ensuring robust, long-term predictive validity.

4.3. Longitudinal model robustness and physical stability

The longitudinal robustness of the global models is fundamentally predicated on the physical and chemical stability of the pharmaceutical matrices. Beyond its utility as a rapid porosity PAT, THz-TDS provides information on the intrinsic material properties such as the

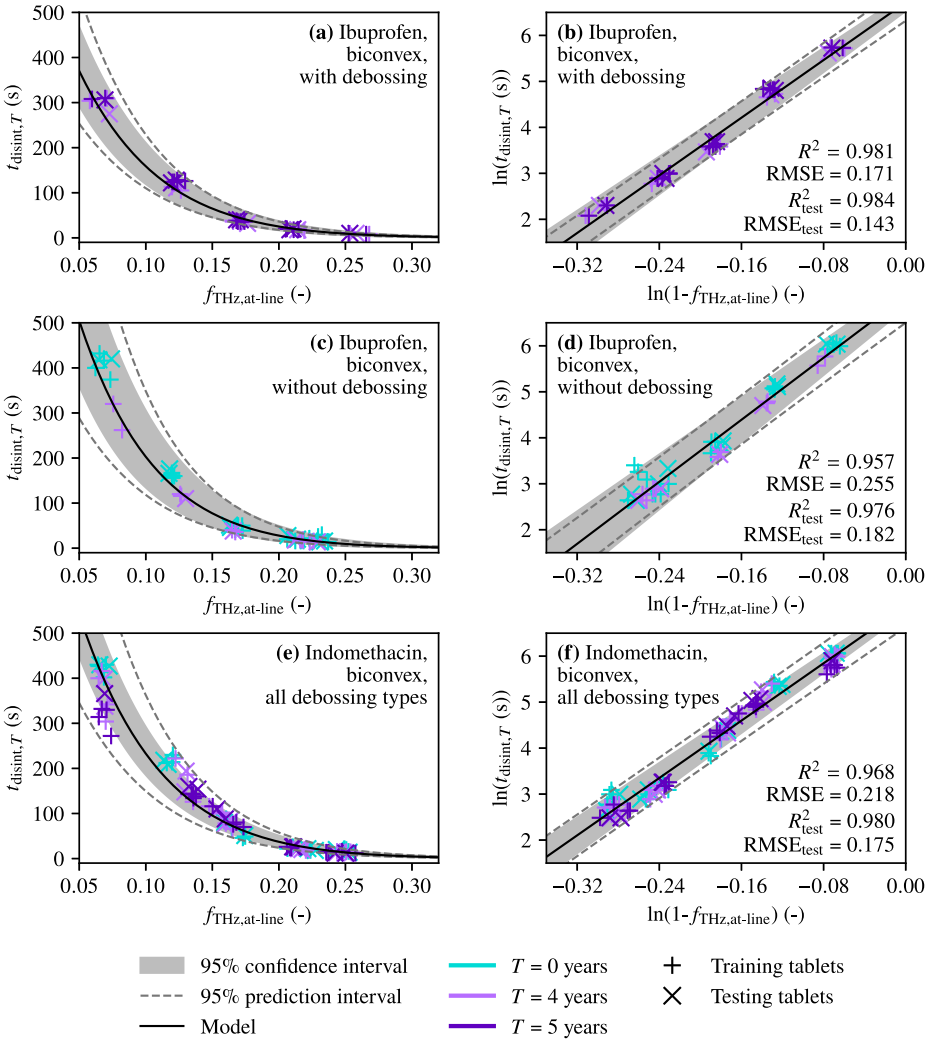

Fig. 3. Global models for disintegration times t_{disint} against the at-line porosity $f_{THz,at-line}$, and the corresponding training and testing data for ibuprofen biconvex tablets (a) with and (c) without debossing, and (e) indomethacin biconvex tablets both with and without debossing. (b, d, f) show the corresponding logarithmic transformations, demonstrating the linear fit of the models. R^2 and RMSE values are resulted from fitting the training data to the respective models. R^2_{test} and $RMSE_{test}$ evaluate the agreement of the testing data with the corresponding models.

solid refractive index $n_{solid}(\nu)$ and absorption coefficient $\alpha_{solid}(\nu)$ spectra (Fig. 6). For all investigated tablet types, $\alpha_{solid}(\nu)$ remained consistent over the five-year study period. The monotonically increasing $\alpha_{solid}(\nu)$ spectra correspond to the vibrational density of states (VDOS), and their consistency over time suggests an absence of phase transformations. The absolute accuracy of the extracted $n_{solid}(\nu)$ and $\alpha_{solid}(\nu)$, which are derived from $\hat{n}_{solid}(\nu)$ and thus $\hat{n}_{eff}(\nu)$, is subject to the constraints of the biconvex tablet geometry. $\hat{n}_{eff}(\nu)$ is measured through the tablet centre, which has a higher porosity than the overall f_{nom} [48]. This spatial heterogeneity results in a slight systematic offset in the calculated $\hat{n}_{solid}(\nu)$ from the true value [42]. The slightly different $n_{solid}(\nu)$ determined from tablet types of the same formulation with and without debossing can also be similarly explained by the geometric sensitivity of THz-TDS. Nonetheless, to confirm longitudinal stability, the temporal consistency of these values is more critical than their absolute accuracy. Although $n_{solid}(\nu)$ shifts systematically from the $T = 0$ years spectrum, the results are inconclusive regarding material property alterations due to the overlapping $n_{solid}(\nu)$ ranges observed in Fig. 6a, e.

Since ibuprofen biconvex tablets with and without debossing showed different disintegration kinetics (Sections 4.1 and 4.2), the chemical integrity of the five-year-old ibuprofen formulation was additionally verified via ATR-FTIR spectroscopy (Fig. 7). The infrared spectra of the five-year-old ibuprofen formulation closely align with the freshly prepared formulation (Fig. 7). The characteristic C=O stretching vibration of ibuprofen at approximately 1710 cm^{-1} remains clearly resolved in the five-year-old formulation, consistent with both the fresh formulation and pure ibuprofen scaled to 10 %, equivalent to the ibuprofen mass fraction in the formulation (Fig. 7). The broad absorption bands at 1000 cm^{-1} and 3400 cm^{-1} (Fig. 7) correspond to the microcrystalline cellulose (MCC) and lactose anhydrous in the formulation [49,50]. The chemical stability of the ibuprofen formulation is confirmed. These results further provide evidence that the distinct k and r parameters, and hence the different disintegration kinetics, observed for ibuprofen biconvex tablets with and without debossing are attributed to geometric factors rather than chemical alterations.

THz-TDS measurements also allow determination of the depolarisation factor L, providing information on the pore shape. Although an analysis of L would be beneficial, prior work has demonstrated that L can only be reliably isolated in tablets with uniform porosity distributions, from which the biconvex tablets in this study deviate [42]. Determining the precise impact of debossing on the pore shape and thus model parameters k and r in ibuprofen biconvex tablets will necessitate further investigation using complementary techniques.

The longitudinal applicability of constant model parameters k and r within the global models is predicated upon the physicochemical stability of the formulation. Furthermore, the temporal stability of these

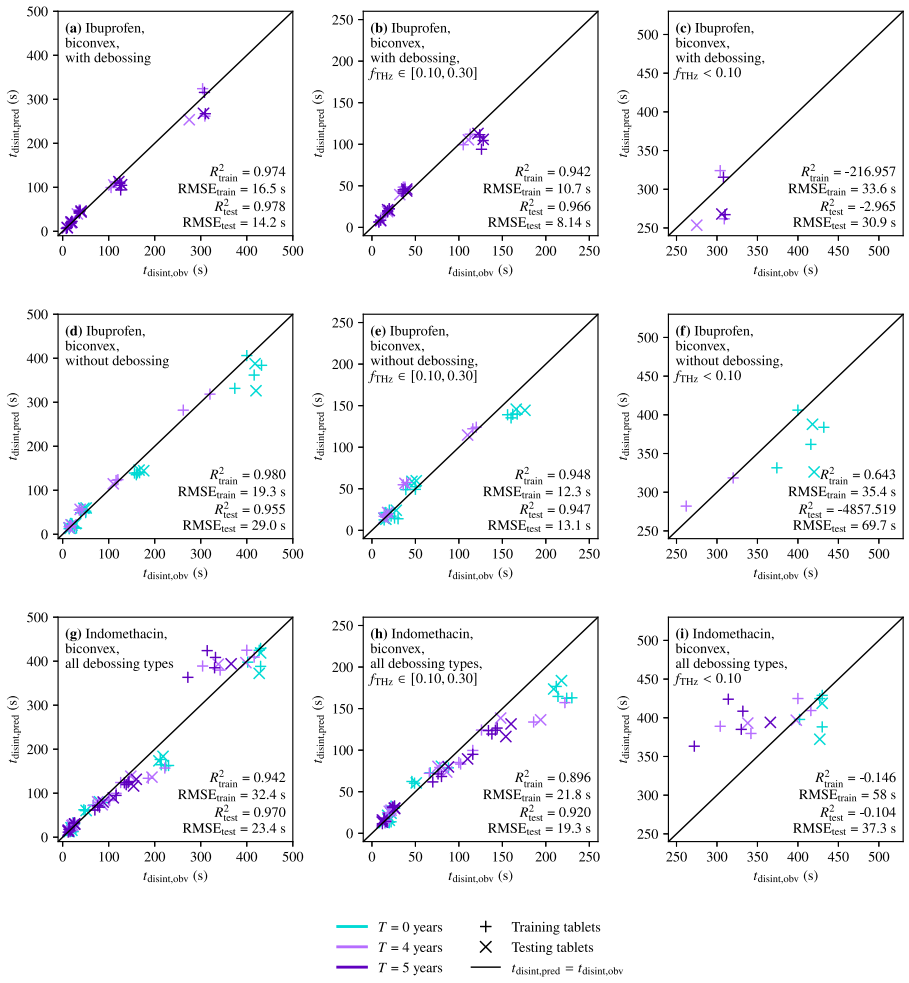

Fig. 4. Agreement between predicted $t_{disint,pred}$ and observed $t_{disint,obv}$ disintegration times of ibuprofen biconvex tablets (a, b, c) with and (d, e, f) without debossing, and (g, h, i) indomethacin biconvex tablets both with and without debossing. (a, d, g) display all results, (b, e, h) display the results within the model operating range ($f_{THz} \in [0.1, 0.3]$), whereas (c, f, i) show results below the operating space ($f_{THz} < 0.1$). $t_{disint,pred}$ are derived from the global models.

parameters supports the hypothesis that $f_{at-line}$ is the dominant CQA governing disintegration, yielding a functionally robust and longitudinally valid model. The negligible impact of Δf over time on k and r suggests that the dynamic evolution of the pore structure is sufficiently encapsulated within the model's hybrid architecture. Future studies should expand this model to a broader range of formulations and manufacturing processes to further establish model universality and explore the mechanistic derivations of k and r. Moreover, evaluating a larger cohort of testing tablets with a broader porosity range than the training set will more robustly validate the model's predictive capability and demonstrate its industrial readiness.

4.4. Strategic selection of process analytical technology

While the proposed hybrid model is fundamentally agnostic to the method of porosity characterisation, its industrial efficacy is maximised when paired with a high-fidelity, rapid and non-destructive PAT. In this study, THz-TDS was selected for its established capability for both at-line and in-line pharmaceutical monitoring [34,39]. THz-TDS is a rapid, non-contact and deterministic PAT capable of simultaneous multi-attribute quantification. Beyond porosity, it has been robustly validated for the assessment of tablet mass, thickness, breaking force, absence of crystallinity, disintegration and dissolution time [30–34, 36,38,39,51–53]. The successful integration of the simple longitudinal disintegration model with THz-TDS further establishes THz-TDS's capability and effectiveness as a multi-attribute PAT. More importantly, the model's ease of implementation within existing digital-manufacturing architectures is demonstrated.

4.5. Industrial utility and life-cycle management

The simple hybrid model presented herein offers a robust approach for disintegration prediction across the entire OSD life cycle, from initial formulation development to commercial manufacturing. While traditional disintegration studies focus primarily on the immediate impact of critical material attributes and process parameters [2,4,6,7], this model prioritises clinical relevance by linking at-line structural data to point-of-care performance.

4.5.1. Quality by design and stability prediction

In the context of QbD and Quality by Digital Design (QbDD), this model serves as a predictive tool for the QTPP. The model's simple architecture suggests an easy adaptation to formulations with different properties such as hygroscopicity through determining k and r from experimental data. By establishing the relationship between at-line porosity and longitudinal disintegration early in development, formulators can define a design space that ensures compliant performance throughout the product's shelf life.

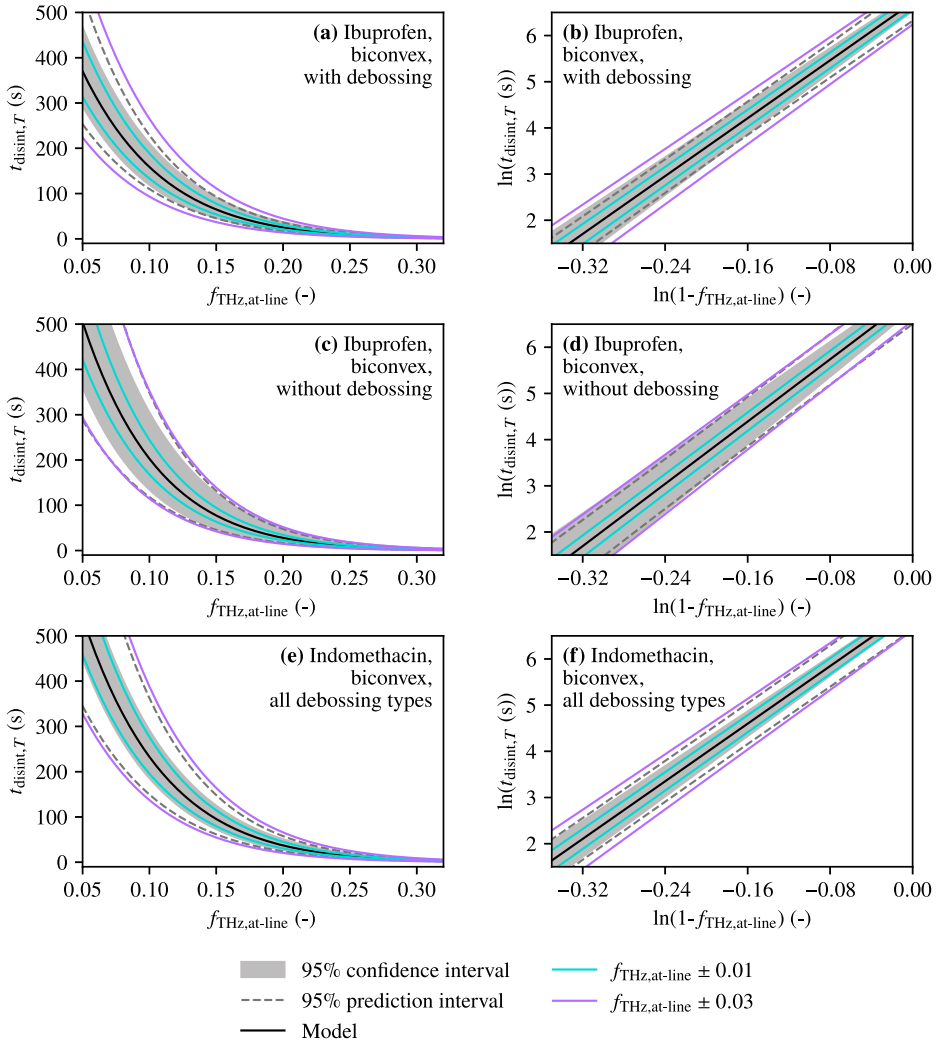

Fig. 5. Sensitivity analysis of the global models for ibuprofen biconvex tablets (a) with and (c) without debossing, and (e) indomethacin biconvex tablets both with and without debossing. The resultant $t_{disint,T}$ predictions under $f_{at-line}$ deviations of ±0.01 and ±0.03 are overlaid against the model, the 95 % confidence interval and the 95 % prediction interval. (b, d, f) present the corresponding logarithmically transformed results.

The current study's five-year real-time stability dataset supports model development and prediction using data from long term and intermediate stability testing. Since accelerated stability studies and the Accelerated Stability Assessment Program (ASAP) are used to predict long-term drug product changes and establish the product shelf life within a shorter time period, the samples and data could also be utilised to establish the model in predicting disintegration times up to and beyond the inferred shelf life. This enables rapid iterations during the Chemistry, Manufacturing and Controls (CMC) development phase.

The acute sensitivity of the hybrid predictive model (Section 4.2) demonstrates its capacity to readily detect subtle, latent alterations that may manifest in less stable formulations. Statistically significant drifts in the parameters k or r over the shelf life can efficiently capture systematic changes in disintegration driven by underlying instabilities such as microstructural relaxation, solid-state transformations or chemical degradation. Whereas in a stable system, the parameters remain invariant over time as demonstrated in Sections 4.1 and 4.2. The insights into the impact of critical attributes on long-term performance not only enables accurate $t_{disint,T}$ prediction but also directly facilitates QbD paradigms in drug product development.

4.5.2. Operational efficiency and technology transfer

The simplicity of the hybrid approach facilitates seamless technology transfer between drug product development and manufacturing. Unlike complex artificial intelligence or machine learning models, which typically require massive datasets and "black-box" validation, this model is physically explainable and requires significantly fewer experimental inputs. This reduction in data dependency simplifies model maintenance and regulatory filing.

When integrated into manufacturing, the model transforms a porosity PAT into a soft sensor for point-of-care disintegration monitoring. This capability enables clinically relevant quality control and RTRT, while reducing reliance on destructive pharmacopoeial end-product testing and accelerating batch release cycles.

4.5.3. Product life-cycle management

The model's flexibility extends to product life-cycle management. Should minor formulation adjustments or equipment changes occur, the model can be rapidly recalibrated or validated with minimal resource expenditure. By linking tablet structure to disintegration through a simple mechanistically grounded framework, this model is pragmatic and flexible. Both predictive quality assurance and longitudinal performance transparency is thus ensured.

CQAs monitored at-line can then be verified with high confidence that they are maintained throughout the shelf life and up to the point-of-care.

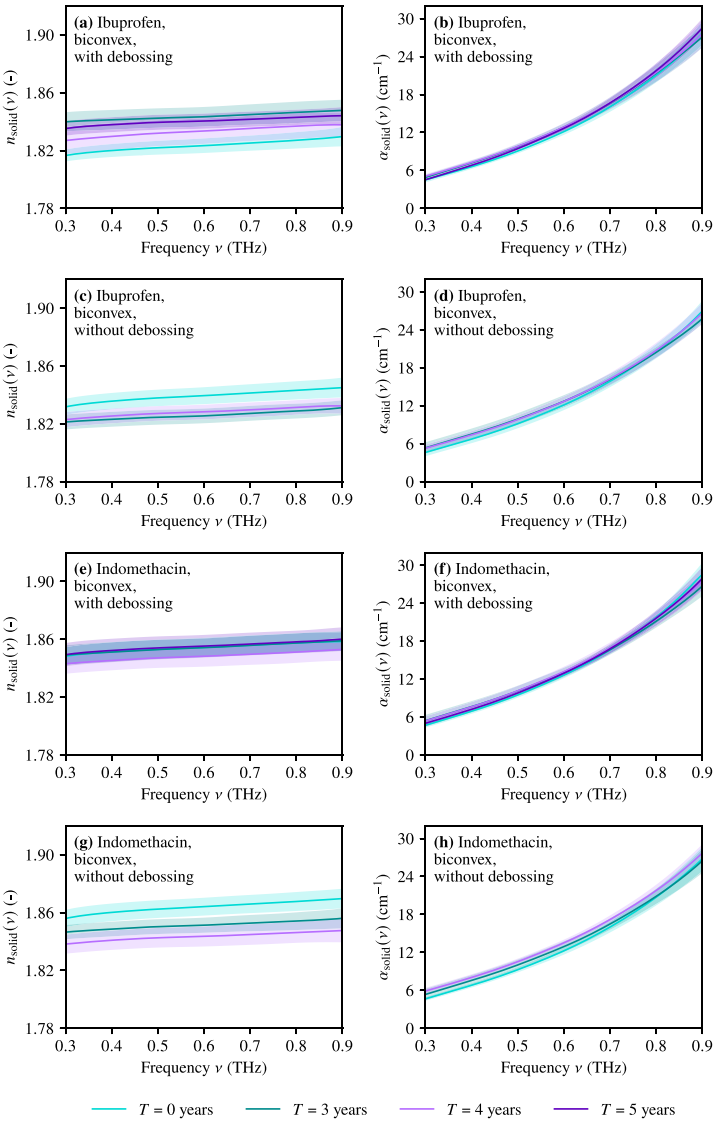

Fig. 6. Solid refractive index $n_{solid}(\nu)$ and absorption coefficient $\alpha_{solid}(\nu)$ spectra for ibuprofen biconvex tablets (a, b) with and (c, d) without debossing, and indomethacin biconvex tablets (e, f) with and (g, h) without debossing. The shaded area indicates the standard deviation.

5. Conclusion

Disintegration is a performance-controlling process for immediate-release (IR) oral solid dosage (OSD) forms, making its quantification a critical component of the Quality Target Product Profile. While porosity is established as a dominant critical quality attribute (CQA) governing disintegration, a gap remains in relating at-line structural measurements to point-of-care performance.

To address this, a simple hybrid model that predicts longitudinal disintegration times $t_{disint,T}$ based on the at-line porosity $f_{at-line}$ is established. The model is anchored in United States Pharmacopoeia ⟨701⟩ disintegration testing to ensure regulatory compliance and reproducibility, while maintaining an architecture agnostic to specific porosity characterisation. To reduce dimensional complexity, other contributing factors are encapsulated within two data-driven parameters: r, which represents mass transport and bond-breakage thresholds, and k, which subsumes these effects while capturing fluid–solid interactions and particle detachment.

Using a unique five-year real-time stability dataset, global models for ibuprofen and indomethacin formulations are established, achieving exceptional predictive accuracy ($R^2 > 0.92$) across all longitudinal time points. An operating range was established within $f_{at-line} \in [0.1, 0.3]$, matching typical porosities of commercial pharmaceutical OSDs. The model effectively captures the impact of debossing on the disintegration performance of ibuprofen biconvex tablets, whilst indomethacin biconvex tablets were negligibly affected. The longitudinal validity of the model and the consistency of k and r over five years are predicated on the physicochemical stability of the investigated formulations. Structural or chemical changes would be informed by deviations in k or r, which result from the acute sensitivity of the model.

The simplicity and adaptability of the model offer a pragmatic path for demonstrating IR OSD efficacy at the point-of-care, in contrast to traditional, destructive end-point testing. By mechanistically relating at-line porosity to point-of-care disintegration performance and detecting systematic changes over time, the model facilitates Quality by Design in drug product development, seamless technology transfer to manufacturing, robust real-time release testing, and flexible and efficient product life-cycle management. Future studies should focus on validating the universal robustness of the model. A broader spectrum of IR OSD formulations with systematically varied APIs, excipients and manufacturing processes shall be investigated. Such validation

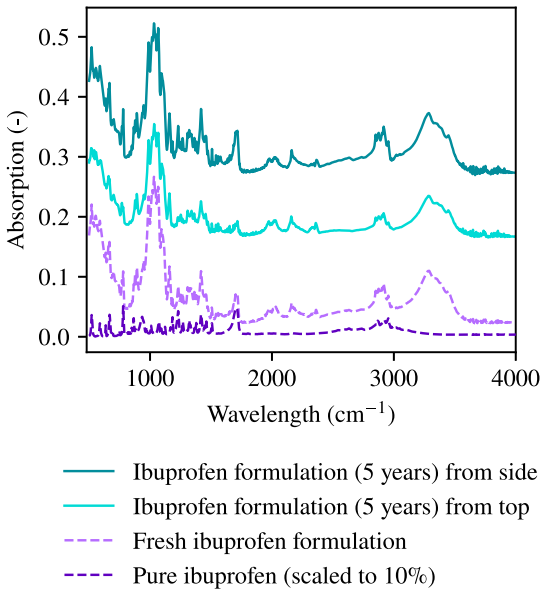

Fig. 7. Infrared spectra of the five-year-old ibuprofen formulation sampled from the container top and side. Reference spectra of a freshly prepared ibuprofen formulation and pure ibuprofen scaled to 10 wt %, equivalent to the mass fraction in the formulation, are presented for comparison. Systematic vertical offsets were applied to the spectra to facilitate visualisation.

is critical, as the current study established a baseline using two formulations with distinct APIs but an identical excipient matrix. The mechanistic derivations of the model parameters shall also be refined to provide more in-depth scientific insights. Ultimately, the simple hybrid predictive model ensures the designed quality and rigorous standards of IR OSDs are demonstrably preserved until the moment of patient administration.

CRediT authorship contribution statement

Chi Ki Leung: Writing – review & editing, Writing – original draft, Visualization, Validation, Software, Methodology, Investigation, Formal analysis, Data curation, Conceptualization. **Prince Bawuah:** Writing – review & editing, Investigation, Data curation. **Nicolas Spiesshofer:** Writing – review & editing, Investigation, Formal analysis, Data curation. **Andreas Kottlan:** Writing – review & editing, Project administration. **Jeremy J. Baumberg:** Writing – review & editing, Supervision. **J. Axel Zeitler:** Writing – review & editing, Supervision, Project administration, Funding acquisition.

Declaration of Generative AI and AI-assisted technologies in the writing process

During the preparation of this work, the author(s) used Gemini by Google in order to improve language. After using this tool/service, the author(s) reviewed and edited the content as needed and take(s) full responsibility for the content of the published article.

Funding sources

RCPE is funded within the framework of COMET – Competence Centers for Excellent Technologies by BMK, BMAW, Land Steiermark, and SFG.

Acknowledgements

CKL acknowledges Research Center Pharmaceutical Engineering GmbH (RCPE), Austria for PhD funding within the K1 PAT-RTRT project consortium. NS acknowledges support from EPSRC Grant EP/L015889/1 for the EPSRC Centre for Doctoral Training in Sensor Technologies and Applications, and from AstraZeneca (MedImmune Ltd).

Appendix A. Details of terahertz time-domain spectroscopy data processing

Each terahertz time-domain spectroscopy (THz-TDS) measurement was acquired from 20 (year 0) or 50 (years 3, 4 and 5) averages at 15 Hz. The time-domain terahertz measurements were then fast Fourier transformed into the frequency domain using a Hann window with a half-width of 10 ps and a 2^2 upsampling factor. The half-width and upsampling factor were minimised whilst ensuring critical pulse features were preserved, and optimal results were reached. Phases were unwrapped at the frequency $\nu = 0.3$ THz and the phase offset was determined from $\nu = 0.2$ THz to 0.4 THz. The complex effective refractive index spectrum $\hat{n}_{\mathrm{eff}}(\nu)$ of the pharmaceutical tablet can then be determined using the tutorial by Leung et al. [54]. The real effective refractive index spectra $n_{\mathrm{eff}}(\nu)$ is given by:

$$n_{\mathrm{eff}}(\nu) = \frac{c_0 \Delta\theta(\nu)}{2\pi\nu H} + n_{\mathrm{air}} \tag{A.1}$$

where ν is the frequency, c_0 is the speed of light in vacuum, $\Delta\theta(\nu)$ is the phase difference between the tablet and baseline measurement and $n_{\mathrm{air}} = 1$ is the refractive index of air. The terahertz data processing was conducted using the THzPy package [55,56] from the dotTHz project [57], and details of the processing are outlined in Leung et al. [54]. The effective refractive index of the pharmaceutical tablet n_{eff} is determined by averaging $n_{\mathrm{eff}}(\nu)$ from $\nu = 0.4$ THz to 0.8 THz, the dynamic range that gives near-constant spectra for all pharmaceutical tablets (Fig. A.1). Herein, n denotes the scalar refractive index, whereas $n(\nu)$ and $\hat{n}(\nu)$ refer to the real and complex refractive index spectra, respectively.

The anisotropic Bruggeman effective medium approximation (AB-EMA) was implemented to determine the terahertz porosity f_{THz}:

$$\frac{n_{\mathrm{solid}}^2 - n_{\mathrm{eff}}^2}{n_{\mathrm{eff}}^2 + L\left(n_{\mathrm{solid}}^2 - n_{\mathrm{eff}}^2\right)}\left(1 - f_{\mathrm{THz}}\right) + \frac{n_{\mathrm{air}}^2 - n_{\mathrm{eff}}^2}{n_{\mathrm{eff}}^2 + L\left(n_{\mathrm{air}}^2 - n_{\mathrm{eff}}^2\right)} f_{\mathrm{THz}} = 0 \tag{A.2}$$

where n_{solid} is the solid refractive index of the formulation, a material property, and L is the depolarisation factor. The AB-EMA can be applied to the scalar refractive indices, real and complex refractive index spectra. Due to the diminishing tablet availability and the possible, though unlikely, chemical degradation over time, L was estimated using the tablets' f_{nom} and n_{eff} for each set to ensure robustness. Since $L \in [0, 1]$, 1001 values within the range were evaluated to identify the optimal L that gives the lowest standard deviation in n_{solid} across all

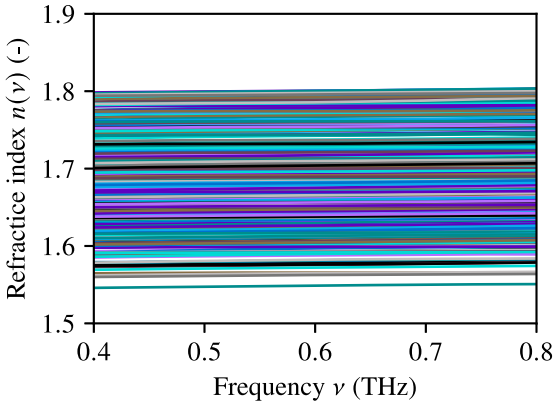

Fig. A.1. Effective refractive index spectra $n_{\mathrm{eff}}(\nu)$ from all THz-TDS measurements of pharmaceutical tablets.

tablets within each set. Using the optimal L for each set, f_{nom} and $\hat{n}_{\text{eff}}(\nu)$ of the tablets, the mean $\hat{n}_{\text{solid}}(\nu)$ is determined for each set. It should be noted that L is simply used here to determine $\hat{n}_{\text{solid}}(\nu)$ and L carries no physical meaning due to the non-uniform porosity distribution in the investigated biconvex tablets [42]. f_{THz} can then be determined with the corresponding $\hat{n}_{\text{eff}}(\nu)$, $\hat{n}_{\text{solid}}(\nu)$ and the optimal L. Whilst the above analysis using the AB-EMA can be implemented via the scalar refractive indices throughout, the complex refractive index spectrum was applied where possible to achieve a more complete analysis at minimal additional computational cost. Further details on the theory of THz-TDS porosity measurements can be found in Bawuah et al. [30].

Appendix B. Additional information on pharmaceutical tablet porosities

The change in the porosity of tablets over time is shown in Fig. B.1 and B.2. The excellent agreement between terahertz f_{THz} and nominal f_{nom} porosity is demonstrated in Fig. B.3.

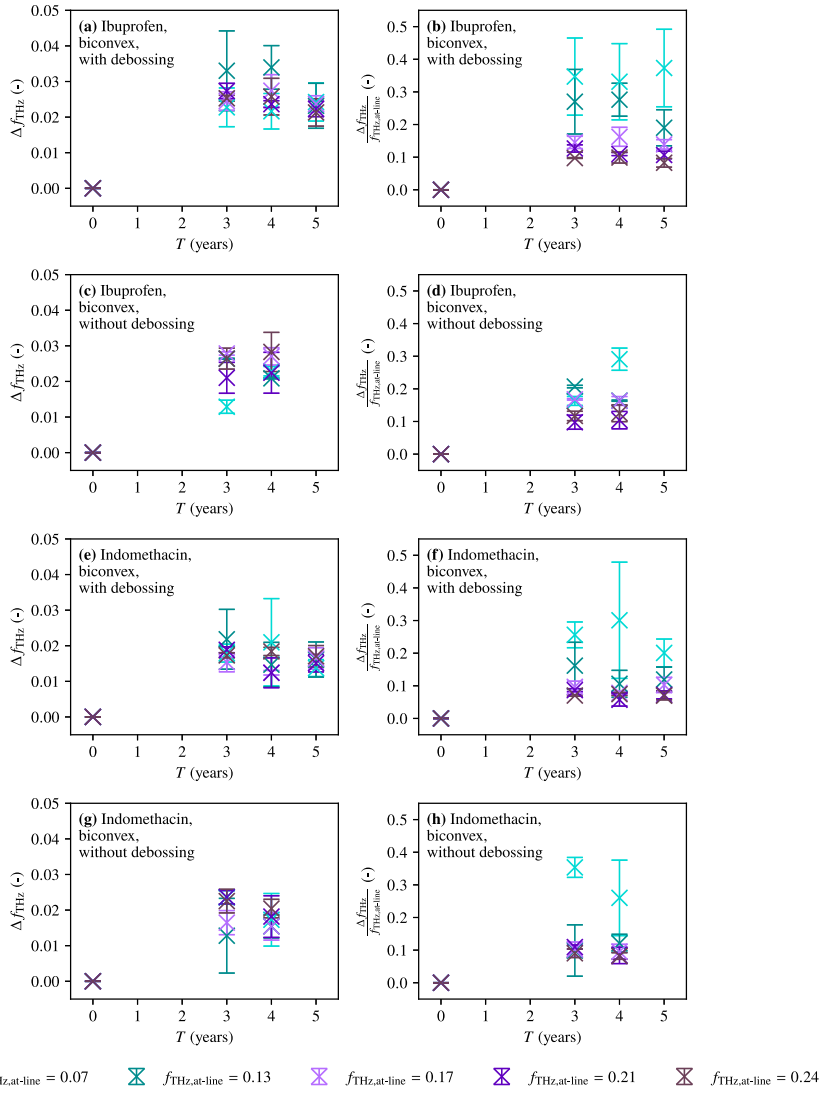

Fig. B.1. Mean change and mean fractional change in porosity f_{THz} over time with respect to the at-line porosity $f_{\text{thz,at-line}}$ for ibuprofen biconvex tablets (a, b) with and (c, d) without debossing, and indomethacin biconvex tablets (e, f) with and (g, h) without debossing. The legend shows the mean $f_{\text{thz,at-line}}$ for each tablet batch.

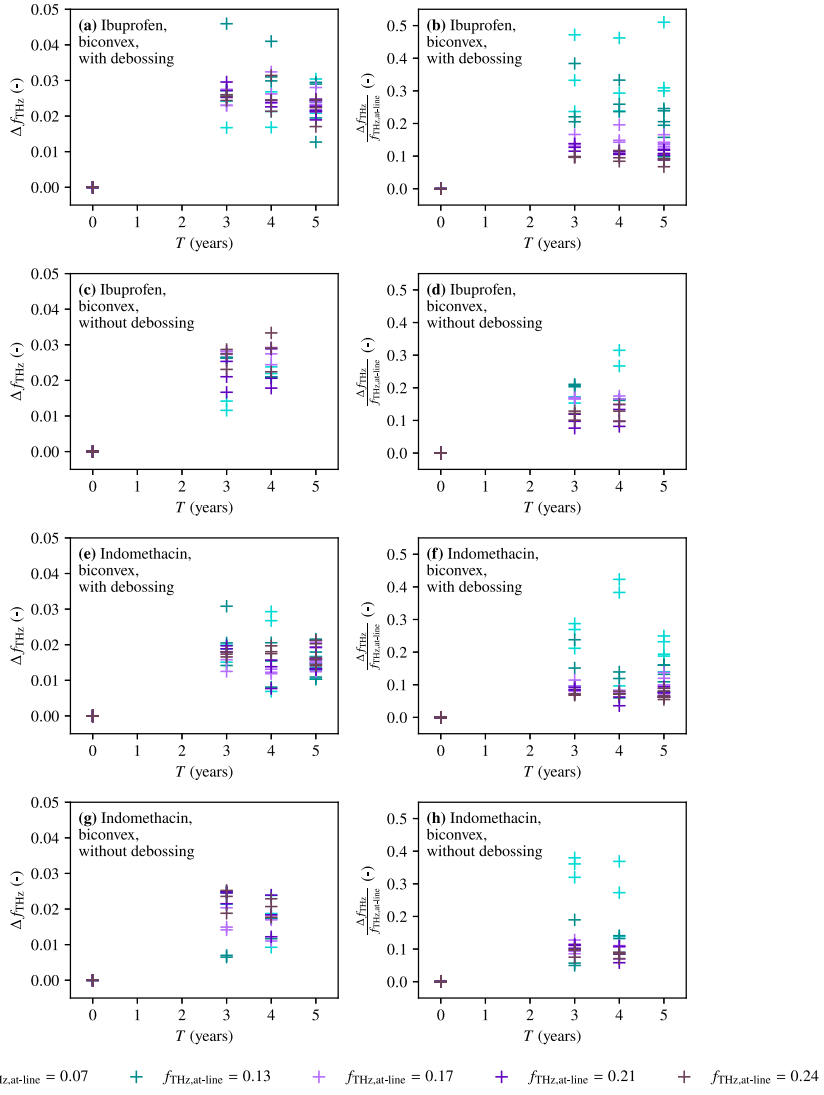

Fig. B.2. Change and fractional change in porosity f_{THz} over time with respect to the at-line porosity $f_{\mathrm{thz,at-line}}$ for individual ibuprofen biconvex tablets (a, b) with and (c, d) without debossing, and indomethacin biconvex tablets (e, f) with and (g, h) without debossing. The legend shows the mean $f_{\mathrm{thz,at-line}}$ for each tablet batch.

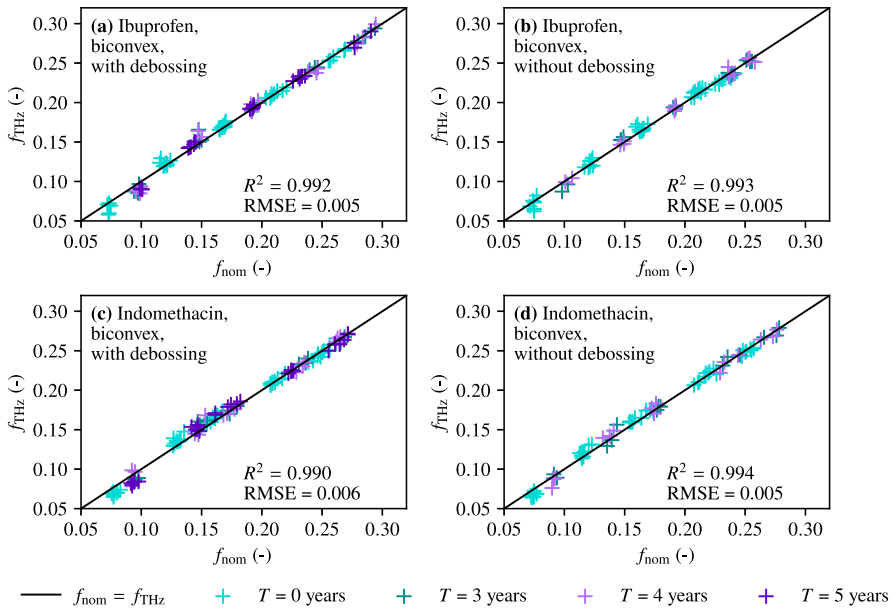

Fig. B.3. Agreement between terahertz f_{THz} and nominal f_{nom} porosities for ibuprofen biconvex tablets (a) with and (b) without debossing, and (c) indomethacin biconvex tablets both with and without debossing.

Data availability

Data will be made available on request.

References

[1] D. Wilson, S. Wren, G. Reynolds, Linking dissolution to disintegration in immediate release tablets using image analysis and a population balance modelling approach, Pharm. Res. 29 (2012) 198–208, http://dx.doi.org/10.1007/s11095-011-0535-1.

[2] D. Markl, J.A. Zeitler, A review of disintegration mechanisms and measurement techniques, Pharm. Res. 34 (2017) 890–917, http://dx.doi.org/10.1007/s11095-017-2129-z.

[3] B. Nickerson, A. Kong, P. Gerst, S. Kao, Correlation of dissolution and disintegration results for an immediate-release tablet, J. Pharm. Biomed. Anal. 150 (2018) 333–340, http://dx.doi.org/10.1016/j.jpba.2017.12.017.

[4] C.G. Jange, C.R. Wassgren, K. Ambrose, The significance of tablet internal structure on disintegration and dissolution of immediate-release formulas: a review, Powders 2 (2023) 99–123, http://dx.doi.org/10.3390/powders2010008.

[5] International Conference on Harmonisation, Specifications: test procedures and acceptance criteria for new drug substances and new drug products: chemical substances, 1999, https://database.ich.org/sites/default/files/Q6A%20Guideline.pdf, (Accessed 02 April 2026).

[6] A. Berardi, L. Bisharat, J. Quodbach, S.A. Rahim, D.R. Perinelli, M. Cespi, Advancing the understanding of the tablet disintegration phenomenon–an update on recent studies, Int. J. Pharm. 598 (2021) 120390, http://dx.doi.org/10.1016/j.ijpharm.2021.120390.

[7] J. Quodbach, P. Kleinebudde, A critical review on tablet disintegration, Pharm. Dev. Technol. 21 (2016) 763–774, http://dx.doi.org/10.3109/10837450.2015.1045618.

[8] J. Cai, T. Jin, J. Kou, S. Zou, J. Xiao, Q. Meng, Lucas–washburn equation-based modeling of capillary-driven flow in porous systems, Langmuir 37 (2021) 1623–1636, http://dx.doi.org/10.1021/acs.langmuir.0c03134.

[9] J. Quodbach, P. Kleinebudde, Systematic classification of tablet disintegrants by water uptake and force development kinetics, J. Pharm. Pharmacol. 66 (2014) 1429–1438, http://dx.doi.org/10.1111/jphp.12276.

[10] N. Maclean, E. Walsh, M. Soundaranathan, I. Khadra, J. Mann, H. Williams, D. Markl, Exploring the performance-controlling tablet disintegration mechanisms for direct compression formulations, Int. J. Pharm. 599 (2021) 120221, http://dx.doi.org/10.1016/j.ijpharm.2021.120221.

[11] D. Markl, S. Yassin, D.I. Wilson, D.J. Goodwin, A. Anderson, J.A. Zeitler, Mathematical modelling of liquid transport in swelling pharmaceutical immediate release tablets, Int. J. Pharm. 526 (2017b) 1–10, http://dx.doi.org/10.1016/j.ijpharm.2017.04.015.

[12] C. So, A.S. Narang, C. Mao, Modeling the tablet disintegration process using the finite difference method, J. Pharm. Sci. 110 (2021) 3614–3622, http://dx.doi.org/10.1016/j.xphs.2021.07.001.

[13] M. Kalnỳ, Z. Grof, F. Štěpánek, Microstructure based simulation of the disintegration and dissolution of immediate release pharmaceutical tablets, Powder Technol. 377 (2021) 257–268, http://dx.doi.org/10.1016/j.powtec.2020.08.093.

[14] M. Soundaranathan, M. Al-Sharabi, T. Sweijen, P. Bawuah, J.A. Zeitler, S.M. Hassanizadeh, K. Pitt, B.F. Johnston, D. Markl, Modelling the evolution of pore structure during the disintegration of pharmaceutical tablets, Pharmaceutics 15 (2023) 489, http://dx.doi.org/10.3390/pharmaceutics15020489.

[15] I. Akseli, J. Xie, L. Schultz, N. Ladyzhynsky, T. Bramante, X. He, R. Deanne, K.R. Horspool, R. Schwabe, A practical framework toward prediction of breaking force and disintegration of tablet formulations using machine learning tools, J. Pharm. Sci. 106 (2017) 234–247, http://dx.doi.org/10.1016/j.xphs.2016.08.026.

[16] R. Han, Y. Yang, X. Li, D. Ouyang, Predicting oral disintegrating tablet formulations by neural network techniques, Asian J. Pharm. Sci. 13 (2018) 336–342, http://dx.doi.org/10.1016/j.ajps.2018.01.003.

[17] M. Momeni, M. Afkanpour, S. Rakhshani, A. Mehrabian, H. Tabesh, A prediction model based on artificial intelligence techniques for disintegration time and hardness of fast disintegrating tablets in pre-formulation tests, BMC Med. Inform. Decis. Mak. 24 (2024) 88, http://dx.doi.org/10.1186/s12911-024-02485-4.

[18] D. Gupta, A.A. Biswas, R.C. Sahu, S. Arora, D. Kumar, A.K. Agrawal, Advancing pharmaceutical intelligence via computationally prognosticating the in-vitro parameters of fast disintegration tablets using machine learning models, Eur. J. Pharmaceut. Biopharmaceut. 204 (2024) 114508, http://dx.doi.org/10.1016/j.ejpb.2024.114508.

[19] A. Moin, F. Fatima, F. Alqahtani, Z.A.A. Asiri, N.A. abo Sahba, H.S. Alqahtani, L.H. Al-Rubaie, U. Hani, Development of machine learning models for estimation of disintegration time on fast-disintegrating tablets, Eur. J. Pharm. Sci. 211 (2025) 107141, http://dx.doi.org/10.1016/j.ejps.2025.107141.

[20] M. Ghazwani, U. Hani, Determination of disintegration time using formulation data for solid dosage oral formulations via advanced machine learning integrated optimizer models, Sci. Rep. 15 (2025) 30118, http://dx.doi.org/10.1038/s41598-025-15996-5.

[21] J. Lee, J. Hancock, D.J. Goodwin, R.M. Dhenge, J. Nassar, J.A. Zeitler, A mechanistic framework for predicting tablet disintegration: Integrating the representative capillary evolution model (rcem) and the dynamic void fraction evolution model (dvfem), Int. J. Pharm. (2025a) 126275, http://dx.doi.org/10.1016/j.ijpharm.2025.126275.

[22] M. Riippi, O. Antikainen, T. Niskanen, J. Yliruusi, The effect of compression force on surface structure, crushing strength, friability and disintegration time of erythromycin acistrate tablets, Eur. J. Pharmaceut. Biopharmaceut. 46 (1998) 339–345, http://dx.doi.org/10.1016/S0939-6411(98)00043-5.

[23] N. Zaborenko, Z. Shi, C.C. Corredor, B.M. Smith-Goettler, L. Zhang, A. Hermans, C.M. Neu, M.A. Alam, M.J. Cohen, X. Lu, et al., First-principles and empirical approaches to predicting in vitro dissolution for pharmaceutical formulation and process development and for product release testing, AAPS J. 21 (2019) 32, http://dx.doi.org/10.1208/s12248-019-0297-y.

[24] J. Quodbach, P. Kleinebudde, Performance of tablet disintegrants: impact of storage conditions and relative tablet density, Pharm. Dev. Technol. 20 (2015) 762–768, http://dx.doi.org/10.3109/10837450.2014.920357.
[25] S. Yassin, D.J. Goodwin, A. Anderson, J. Sibik, D.I. Wilson, L.F. Gladden, J.A. Zeitler, The disintegration process in microcrystalline cellulose based tablets, part 1: influence of temperature, porosity and superdisintegrants, J. Pharm. Sci. 104 (2015) 3440–3450, http://dx.doi.org/10.1002/jps.24544.
[26] A.D. Rajkumar, G.K. Reynolds, D. Wilson, S. Wren, M.J. Hounslow, A.D. Salman, Investigating the effect of processing parameters on pharmaceutical tablet disintegration using a real-time particle imaging approach, Eur. J. Pharmaceut. Biopharmaceut. 106 (2016) 88–96, http://dx.doi.org/10.1016/j.ejpb.2016.06.005.
[27] M. Al-Sharabi, D. Markl, T. Mudley, P. Bawuah, A.P. Karttunen, C. Ridgway, P. Gane, J. Ketolainen, K.E. Peiponen, T. Rades, et al., Simultaneous investigation of the liquid transport and swelling performance during tablet disintegration, Int. J. Pharm. 584 (2020) 119380, http://dx.doi.org/10.1016/j.ijpharm.2020.119380.
[28] W. Jiang, X.Y. Lawrence, Modern pharmaceutical quality regulations: question-based review, Developing Solid Oral Dosage Forms, Elsevier, 2009, pp. 885–901, http://dx.doi.org/10.1016/B978-0-444-53242-8.00038-2.
[29] D. Markl, M. Warman, M. Dumarey, E.L. Bergman, S. Folestad, Z. Shi, L.F. Manley, D.J. Goodwin, J.A. Zeitler, Review of real-time release testing of pharmaceutical tablets: State-of-the art, challenges and future perspective, Int. J. Pharm. 582 (2020) 119353, http://dx.doi.org/10.1016/j.ijpharm.2020.119353.
[30] P. Bawuah, D. Markl, D. Farrell, M. Evans, A. Portieri, A. Anderson, D. Goodwin, R. Lucas, J.A. Zeitler, Terahertz-based porosity measurement of pharmaceutical tablets: a tutorial, J. Infrared, Millim. Terahertz Waves 41 (2020) 450–469, http://dx.doi.org/10.1007/s10762-019-00659-0.
[31] M. Anuschek, T.K. Vilhelmsen, J.A. Zeitler, J. Rantanen, Towards simultaneous determination of tablet porosity and height by terahertz time-domain reflection spectroscopy, Int. J. Pharm. 646 (2023) 123424, http://dx.doi.org/10.1016/j.ijpharm.2023.123424.
[32] M. Anuschek, T.K. Vilhelmsen, J.A. Zeitler, J. Rantanen, Thz-tds transflection measurements as a process analyser for tablet mass, Int. J. Pharm. 666 (2024) 124750, http://dx.doi.org/10.1016/j.ijpharm.2024.124750.
[33] M. Anuschek, A. Nielsen, T.K. Vilhelmsen, J.A. Zeitler, J. Rantanen, Towards real-time process monitoring and control of physical properties of tablets using terahertz spectroscopy, Chem. Eng. Sci. (2025a) 121992, http://dx.doi.org/10.1016/j.ces.2025.121992.
[34] M. Anuschek, T.K. Vilhelmsen, J.A. Zeitler, J. Rantanen, In-line monitoring of tablet compression with terahertz time-domain spectroscopy for physical tablet characteristics, Int. J. Pharm. (2025b) 126273, http://dx.doi.org/10.1016/j.ijpharm.2025.126273.
[35] S. Sacher, A. Kottlan, J.B. Diop, R. Heimsten, Prediction of in-vitro dissolution and tablet hardness from optical porosity measurements, Int. J. Pharm. 660 (2024) 124336, http://dx.doi.org/10.1016/j.ijpharm.2024.124336.
[36] J. Lee, C.K. Leung, L. Gingras, R. Holzwarth, D.J. Goodwin, R.M. Dhenge, J. Nassar, P. Bawuah, J.A. Zeitler, Improved robustness by concurrent rapid and non-destructive terahertz sensing of pharmaceutical tablet thickness and porosity, Int. J. Pharm. (2025b) 125773, http://dx.doi.org/10.1016/j.ijpharm.2025.125773.
[37] R. Brands, T.N. Le, J. Bartsch, M. Thommes, A step towards real-time release testing of pharmaceutical tablets: utilization of cielab color space, Pharmaceutics 17 (2025) 311, http://dx.doi.org/10.3390/pharmaceutics17030311.
[38] P. Bawuah, D. Markl, A. Turner, M. Evans, A. Portieri, D. Farrell, R. Lucas, A. Anderson, D.J. Goodwin, J.A. Zeitler, A fast and non-destructive terahertz dissolution assay for immediate release tablets, J. Pharm. Sci. 110 (2021) 2083–2092, http://dx.doi.org/10.1016/j.xphs.2020.11.041.
[39] P. Bawuah, M. Evans, A. Lura, D.J. Farrell, P.J. Barrie, P. Kleinebudde, D. Markl, J.A. Zeitler, At-line porosity sensing for non-destructive disintegration testing in immediate release tablets, Int. J. Pharm.: X 5 (2023) 100186, http://dx.doi.org/10.1016/j.ijpx.2023.100186.
[40] N. Maclean, J.A. Armstrong, M.A. Carroll, M. Salehian, J. Mann, G. Reynolds, B. Johnston, D. Markl, Flexible modelling of the dissolution performance of directly compressed tablets, Int. J. Pharm. 656 (2024) 124084, http://dx.doi.org/10.1016/j.ijpharm.2024.124084.
[41] C. Sun, A novel method for deriving true density of pharmaceutical solids including hydrates and water-containing powders, J. Pharm. Sci. 93 (2004) 646–653, http://dx.doi.org/10.1002/jps.10595.
[42] M. Anuschek, P. Bawuah, J.A. Zeitler, Terahertz time-domain spectroscopy for powder compact porosity and pore shape measurements: An error analysis of the anisotropic bruggeman model, Int. J. Pharm.: X 3 (2021) 100079, http://dx.doi.org/10.1016/j.ijpx.2021.100079.
[43] DrugBank, Ibuprofen: Uses, interactions, mechanism of action, 2026a, https://go.drugbank.com/drugs/DB01050, (Accessed 02 April 2026).
[44] DrugBank, Indomethacin: Uses, interactions, mechanism of action, 2026b, https://go.drugbank.com/drugs/DB00328, (Accessed 02 April 2026).
[45] H. Van Kamp, G. Bolhuis, K. Kussendrager, C. Lerk, Studies on tableting properties of lactose. iv. dissolution and disintegration properties of different types of crystalline lactose, Int. J. Pharm. 28 (1986) 229–238, http://dx.doi.org/10.1016/0378-5173(86)90249-8.
[46] M. Wewers, S. Czyz, J.H. Finke, E. John, B. Van Eerdenbrugh, M. Juhnke, H. Bunjes, A. Kwade, Influence of formulation parameters on redispersibility of naproxen nanoparticles from granules produced in a fluidized bed process, Pharmaceutics 12 (2020) 363, http://dx.doi.org/10.3390/pharmaceutics12040363.
[47] D. Markl, N. Maclean, J. Mann, H. Williams, A. Abbott, H. Mead, I. Khadra, Tablet disintegration performance: Effect of compression pressure and storage conditions on surface liquid absorption and swelling kinetics, Int. J. Pharm. 601 (2021) 120382, http://dx.doi.org/10.1016/j.ijpharm.2021.120382.
[48] I. Sinka, J. Cunningham, A. Zavaliangos, Analysis of tablet compaction. ii. finite element analysis of density distributions in convex tablets, J. Pharm. Sci. 93 (2004) 2040–2053, http://dx.doi.org/10.1002/jps.20111.
[49] S.M. Doncea, R.M. Ion, R.C. Fierascui, E. Bacalum, A.A. Bunaciu, H.Y. Aboul-Enein, Spectral methods for historical paper analysis: composition and age approximation, Instrum. Sci. Technol. 38 (2009) 96–106, http://dx.doi.org/10.1080/10739140903430271.
[50] National Institute of Advanced Industrial Science, Technology (AIST), Aist: Spectral database for organic compounds, sdbs, 2022, https://sdbs.db.aist.go.jp/CompoundView.aspx?sdbsno=53551, (Accessed 02 April 2026).
[51] D. Markl, J. Sauerwein, D.J. Goodwin, S. Van Den Ban, J.A. Zeitler, Non-destructive determination of disintegration time and dissolution in immediate release tablets by terahertz transmission measurements: Markl et al., Pharm. Res. 34 (2017a) 1012–1022, http://dx.doi.org/10.1007/s11095-017-2108-4.
[52] C.K. Leung, L. Kuchler, J.A. Zeitler, Detecting absence of crystallinity in solid dosage forms with at-line terahertz process analytical technology, Int. J. Pharm. 689 (2026b) 126447, http://dx.doi.org/10.1016/j.ijpharm.2025.126447.
[53] C.K. Leung, L. Kuchler, A. Kottlan, J.A. Zeitler, Physical stability of salbutamol amorphous solid dispersion tablets measured by terahertz spectroscopy, Int. J. Pharm. 697 (2026a) 126903, http://dx.doi.org/10.1016/j.ijpharm.2026.126903.
[54] C.K. Leung, J.N. Ward-Berry, E. Wanvig i Dot, J. Lee, J.A. Zeitler, Tutorial: Accurate determination of refractive index and absorption coefficient in terahertz time-domain spectroscopy, J. Infrared, Millim. Terahertz Waves 46 (2025) 59, http://dx.doi.org/10.1007/s10762-025-01070-8.
[55] J. Ward-Berry, L. Stoeckli, C. Leung, J. Zeitler, Introducing thzpy: An open-source python package for processing terahertz time-domain data, in: 2025 50th International Conference on Infrared, Millimeter, and Terahertz Waves (IRMMW-THz), IEEE, 2025, http://dx.doi.org/10.1109/IRMMW-THz61557.2025.11319635, 1–1.
[56] Terahertz Applications Group, University of Cambridge, Thzpy, 2025, https://github.com/dotTHzTAG/thzpy, (Accessed 14 September 2025).
[57] J. Lee, C.K. Leung, M. Ma, J. Ward-Berry, S. Santitewagun, J.A. Zeitler, The dotthz project: A standard data format for terahertz time-domain data, J. Infrared, Millim. Terahertz Waves 44 (2023) 795–813, http://dx.doi.org/10.1007/s10762-023-00947-w.